Shock compression of semicrystalline polymers

Pedro S. Lance,* Daniel A. Vega, and Leopoldo R. Gómez†
Department of Physics, Universidad Nacional del Sur - IFISUR - CONICET, Bahía Blanca 8000, Argentina

(Received 8 March 2023; revised 21 September 2023; accepted 9 October 2023; published 23 October 2023)

Here, we study the shock wave response of semicrystalline polymers using coarse-grained molecular dynamics simulations. The crystallinity of the systems was controlled by using block copolymer-like chains with different volume fractions of crystallizable blocks. Our results indicate that the degree of initial crystallinity affects the speed of sound and the propagation velocity of shock waves at low compression velocities. However, at high compression velocities, the initial crystalline structures melt due to the passage of the shock, and the principal shock features resemble each other, independently of the crystallinity. We also found that the presence of crystalline regions helps disperse shocks, resulting in a monotonic increase in shock width with the degree of initial crystallinity. The shock-induced melting of crystalline structures was analyzed by an Avrami function, revealing similarities with conventional thermal melting. Our simulation results highlight the importance of crystalline regions and the presence of amorphous/crystal interfaces in contributing to the dispersion and dissipation of shocks and impact fronts traveling through semicrystalline polymeric materials.

DOI: 10.1103/PhysRevMaterials.7.105602

I. INTRODUCTION

Shock waves are powerful events that can have a significant impact on the structural integrity and behavior of materials [1]. When a shock wave suddenly increases pressure on a system, it can cause nonlinear behavior, significant deformations, and even failures, fractures, or phase transitions [2]. As such, there has been a growing interest in understanding how different materials respond to high strain rates.

Recent research suggests that polymeric materials may offer high resistance to impacts [3–6]. Compared to other commonly used shock-absorbing materials, such as metals, polymers possess several advantages, including lower density, controllable transparency, rate-dependent behavior, and self-healing ability, which make them promising candidates for various applications, including protective equipment, transportation, and infrastructure.

Polymer blends, composed of both hard (glassy or crystalline) and soft (amorphous) regions, have emerged as a promising material for blast and impact absorption [5–8]. The combination of hard and soft regions in these materials is expected to effectively disperse shock waves and dissipate impact energy, making them potentially effective at mitigating the harmful effects of explosions and impacts. In these systems, the hard regions in the material are expected to act as a source of shock-wave dispersion, effectively spreading the energy throughout the material and reducing the overall impact. On the other hand, the soft regions would dissipate impact energy by undergoing plastic deformation and absorbing part of the kinetic energy of the impact.

Semicrystalline polymers offer a simple and versatile means of achieving two-phase (hard-soft) systems [9]. By controlling the dynamics of crystallization, it is possible to manage various crystal properties, such as the final degree of crystallization and crystal morphology [9,10]. When no external restrictions are imposed, polymers can crystallize while maintaining amorphous regions due to morphology and geometric constraints. The dynamics of crystallization and final structures have been extensively studied using computer simulations and experiments, revealing that the degree of crystallinity largely affects the mechanical properties of semicrystalline polymers [10].

Block copolymers are another way to create materials with a controlled fraction of hard and soft regions [11]. They are produced by chemically bonding two or more polymer chains together, allowing one block to be composed of hard components and the other to be soft and amorphous. By regulating the volume fraction of each block, the proportion of hard and soft regions in the system can be controlled, leading to materials with precisely tuned mechanical properties, which can be modified by adjusting the length of the blocks, the volume fraction, and the distribution of the blocks in the polymer chains [11].

In this study, we employ coarse-grained molecular dynamics (CG-MD) simulations to investigate the shock compression of semicrystalline polymers with block copolymer-like chains (Fig. 1). By controlling the degree of crystallinity, we analyze the key characteristics of shock propagation through different crystalline systems. Our goal is to investigate how the degree of crystallinity influences the shock-absorbing properties of polymeric materials, which will identify ways to develop materials with superior mechanical properties.

II. METHODS

We conducted CG-MD simulations using LAMMPS [12] to study the shock compression of semicrystalline polymers. Our model is based on poly(vinyl alcohol) (PVA) and was developed by Reith *et al.* [13], who used an atomistic-to-coarse-grained mapping where a coarse-grained

*pedro.lance@uns.edu.ar
†lgomez@uns.edu.ar

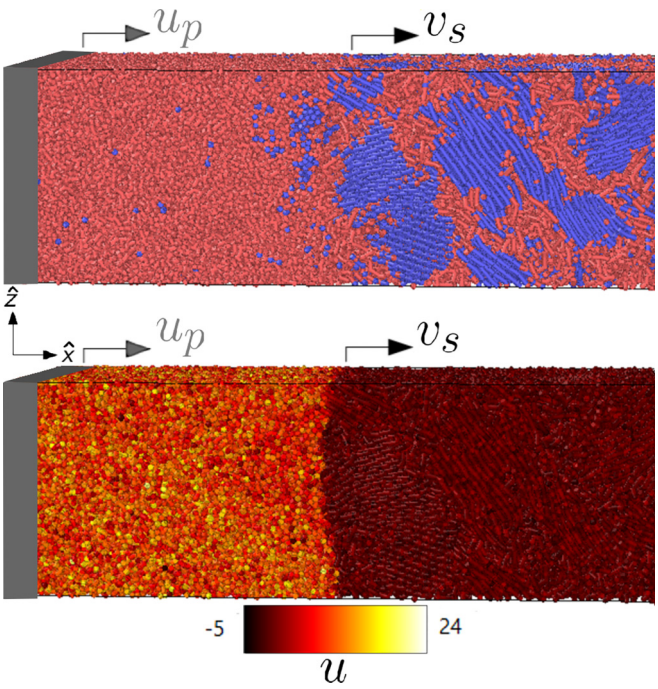

FIG. 1. Dynamic shock compression of semicrystalline polymers. A piston moving at a high velocity u_P compresses the media and generates a shock wave that travels through it at a velocity v_S. Very fast compressions can result in strong shocks that have the potential to melt the crystalline (blue) regions, as seen in the upper panel. The passage of the shock wave can also be visualized through the particle velocity in the compression direction, as shown in the bottom panel.

bead represents one monomeric unit of PVA. This model has been widely utilized in exploring various properties of crystalline polymers [14–17]. Additionally, due to the similar monomer number density and angle bending potential of polyethylene to PVA, this model was also proposed to study the structural and dynamical properties of crystals in polyethylene [15].

The pair interaction between beads in this model is described by a truncated and shifted LJ-96 potential, which is a function of the distance r between the beads:

$$U_{\mathrm{LJ96}} = \begin{cases} 4\epsilon_{96}\left[\left(\frac{\sigma_{96}}{r}\right)^9 - \left(\frac{\sigma_{96}}{r}\right)^6\right] + \delta, & r \leqslant r_c, \\ 0, & r > r_c, \end{cases} \quad (1)$$

where $\epsilon_{96} = 0.37775\epsilon$, $\sigma_{96} = 0.89\sigma$, $r_c = 1.0188\sigma$ is the cut-off distance, and δ is defined in such a way that the potential is shifted to zero at r_c [14,15].

Bond interactions were defined by using a harmonic potential,

$$U_{\mathrm{bond}} = K(r - r_0)^2, \quad (2)$$

where $K = 1352\,\epsilon/\sigma^2$, and $r_0 = 0.5\,\sigma$.

We utilized a tabulated angle potential that includes three minima located at 180°, 126°, and 95°, representing the trans-trans, trans-gauche, and gauche-gauche conformations of the atomistic backbone chain, respectively [13]. Non-bonded interactions were excluded between first and second neighbors along each chain. The degree of polymerization for all systems studied here was $N = 100$. The simulations were conducted using unitless LJ units and $k_b = 1$ was considered. The scaling factors employed were as follows: distance $\sigma = 0.52$ nm, mass $m = 44$ g/mol, temperature $T^* = 550$ K, pressure $P^* = 12662.5$ Pa, and time $\tau = 2$ ps [13].

To generate the initial configurations, a random walk technique was utilized to create chains, which were subsequently relaxed using dissipative particle dynamics (DPD) [18]. NPT simulations were then performed to further relax the systems while maintaining the pressure at a value of $P = 8\epsilon/\sigma^3$ (1 atm) and cooling them to $T = 0.6T^*$ (330 K), which is below the melting point, while periodic boundary conditions were employed.

No external restrictions were imposed during the cooling process, allowing the systems to crystallize freely, leading to grains with varying orientations and trapped amorphous regions. All systems were cooled for a minimum of 10^7 time steps to ensure system equilibrium. To minimize errors caused by random crystal and amorphous region distributions, as well as variations in crystal orientation and morphology, we obtained the results by averaging the measurements obtained from three equivalent systems that were cooled at different rates.

To calculate the crystallinity, χ_0, we analyzed the orientational correlations between bonds. The simulation box was partitioned into subsystems (boxes), and the mean bond orientation was obtained for each box. If the majority of the bond directions in a box were within a certain threshold of the mean bond direction for that box, the bonds were classified as crystalline; otherwise, they were categorized as amorphous. The total crystallinity was calculated as the fraction of crystalline bonds [17,19].

In order to control the degree of crystallinity in the systems, we used block copolymer-like chains in which only a fraction f of the chain had angular interactions, allowing this portion to crystallize at low temperatures. The rest of the chain remained amorphous at all temperatures. In our study, we considered the fraction of crystalline regions to be $f = 0.0$, 0.25, 0.5, and 1.0. Figures 2(a)–2(c) show typical equilibrated semicrystalline systems obtained for fractions $f = 0.25$, 0.5, and 1.0, where the crystalline (amorphous) regions are colored in blue (red). Note that, due to geometric restrictions, the final crystallinity of the system χ is generally smaller than the crystallizable fraction of the chain, as shown in Fig. 2(d). Nonetheless, as expected, this figure shows that the crystallinity increases monotonically when the fraction of crystallizable regions is increased. It is also worth noting that the degree of crystallinity in the systems could be regulated through temperature or cooling rate adjustments. However, modifying the final temperature of the systems would mean subjecting them to compression at varying temperatures, which could influence the propagation of shock waves. Hence, we chose to compress the semicrystalline systems at a consistent temperature, while varying the degree of crystallinity by controlling the fraction f of the polymer chain that could crystallize.

With the initial semicrystalline configurations established, we removed the periodic boundary conditions along the compression axis, simultaneously eliminating any bonds of particles that intersected these planes. The shock wave was

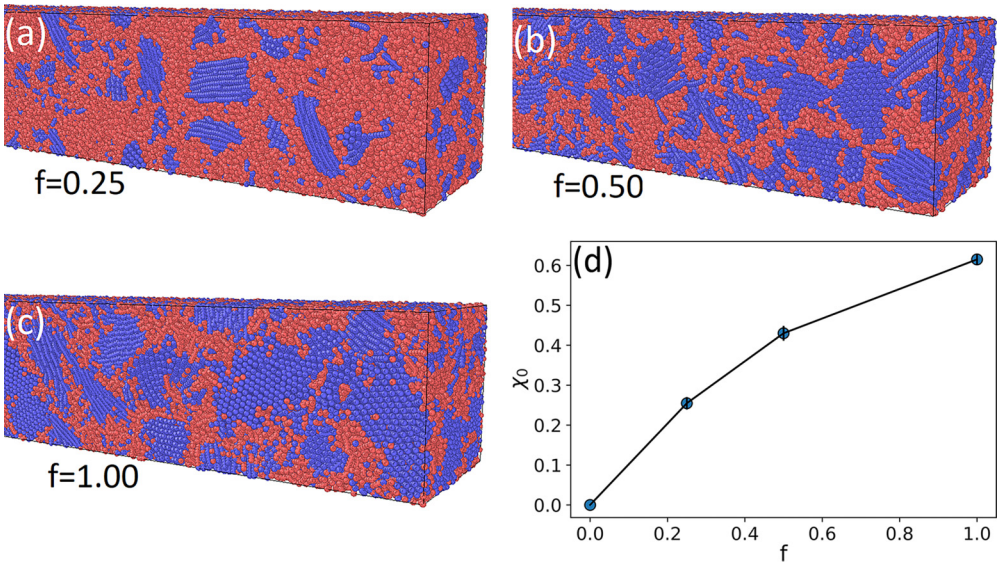

FIG. 2. Modeling semicrystalline polymers. Panels (a)–(c) show equilibrated semicrystalline systems obtained for different values of the fraction of crystallizable chain f. The blue particles correspond to crystalline regions, and the red particles correspond to amorphous regions. Panel (d) shows the crystallinity of the system, χ, after equilibration as a function of the fraction f.

generated using a piston compression simulation in the NVE ensemble, as described in [20]. This process entailed compressing the simulation box at a uniform velocity with the aid of the open-source LAMMPS software [21]. In our simulations, the moving piston effect was simulated by uniformly propelling particles near one end of the box at a constant velocity u_p. Simultaneously, the opposite face of the simulation box remained stationary. This approach gave rise to a sharp wave front traveling at a higher velocity v_s, depicted in Fig. 1. The high velocity of the piston necessitated the use of a smaller time step of $\tau = 5 \times 10^{-6}$.

III. RESULTS

In general, the passage of a shock wave can cause significant distortion to the initial structure of a semicrystalline polymer. This phenomenon is clearly observed in Fig. 3(a), where we present the final pair correlation function in the semicrystalline system, utilizing both crystalline and amorphous particles, after the shock has traversed the material at various compression velocities, denoted as u_p. Initially, at $u_p \equiv 0$, the structure exhibits pronounced high-order peaks due to the presence of crystalline order. However, as the system undergoes dynamic compression, these peaks become distorted, with the first peak shifting to lower values and broadening due to compression. Moreover, with increasing compression velocity, the higher-order peaks progressively broaden and diminish in magnitude, indicating a greater degree of distortion caused by the shock. At the highest compression velocities ($u_p \gtrsim 4$), the crystalline regions even begin to melt, and the shocked structure becomes completely amorphous, with broadened peaks in $g(r)$.

The distortion and melting of crystalline domains resulting from the passage of the shock are further evident from Fig. 3(b), where we depict the pair correlation between crystalline-crystalline and amorphous-amorphous particles. This plot clearly shows that the crystal particles exhibit a higher level of order, as evidenced by the presence of well-defined high-order peaks in the pair correlation of the undistorted system ($u_p = 0$). However, as the system becomes compressed by the piston, the introduction of energy induces distortions in the crystal bonds, leading to the smearing of the high-order peaks in the pair correlation. Additionally, it is worth noting that both crystal-crystal and amorphous-amorphous correlations experience a decrease in the intensity of the dominant peak of $g(r)$ due to compression. This reduction is accompanied by a shift towards smaller distances, as expected.

Figure 1 shows an extreme case where the shock compression of a semicrystalline system with crystallinity $\chi_0 = 0.63$ at velocity $u_p = 9$ leads to the complete melting of the crystalline structure. The melting of the crystalline structures can be observed in the upper panel, where particles are colored according to the local phase. As a result of the energy injection from the passage of the shock front, the initial crystalline regions (represented by blue particles) transition to disordered amorphous structures (represented by red particles). It is worth noting that shock waves can generally be viewed as adiabatic (fast) transitions, which cause the system to heat up and potentially lead to phase transitions and melting [22]. Figure 4 displays the final temperature of the semicrystalline systems as a function of the compression speed, denoted as u_p. As evident from the figure, faster compression results in greater heating. Furthermore, for a specific compression velocity, the temperature rise is less pronounced in systems with higher initial crystallinity. This is because some of the energy introduced by dynamic compression is consumed in melting the crystalline structures. Therefore, in shock waves, phase transformations result from dynamic compression and heating of the system, rather than heat exchange with the surrounding medium.

In the bottom panel of Fig. 1, particles are colored by their velocity in the shock propagation direction (x axis). From this plot, the shock front is easily visualized. As observed in

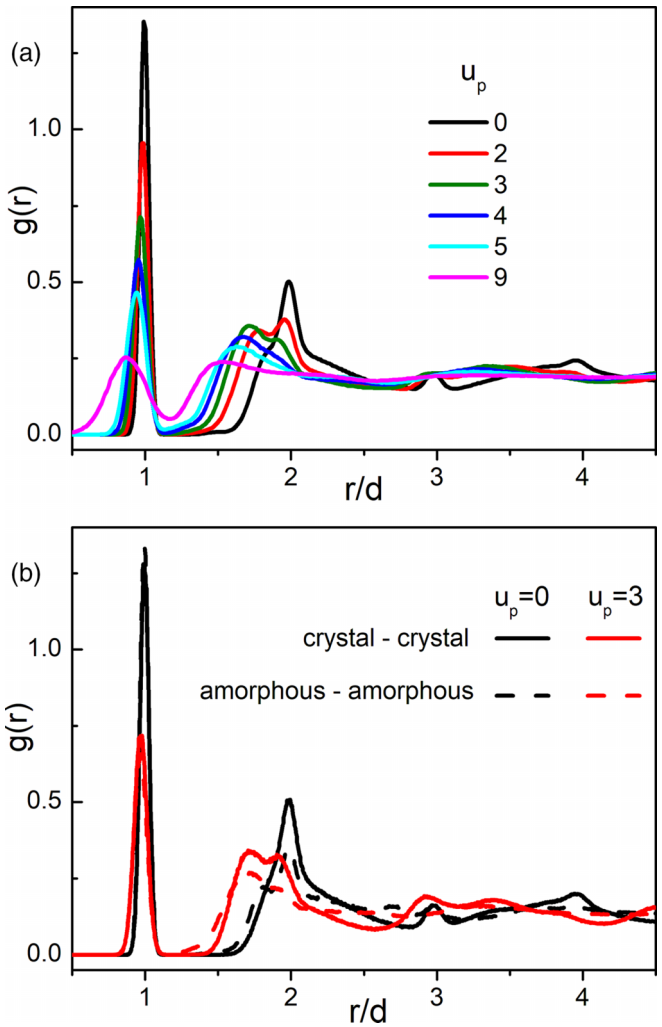

FIG. 3. Structural distortions after shock compression. (a) Pair correlation function in a semicrystalline system after the passage of a shock wave at different compression velocities (u_p). Distortion and melting of crystalline domains are observed as peaks shift, broaden, and disappear. (b) Pair correlation between crystalline-crystalline and amorphous-amorphous particles, showing distortion of crystal bonds and reduced peak intensity due to compression.

other systems, we found that the uniform compression of a semicrystalline polymer at velocity u_p leads to the formation of a shock front that steadily propagates throughout the system at a higher velocity, v_s. Here, we used the velocity of particles to track the position of the front through time and to obtain the shock velocity v_s for different compression velocities u_p and systems with different degrees of crystallinity χ_0.

Figure 5(a) shows the shock velocity v_s as a function of the compression velocity u_p for systems of different crystallinity. Note that, at high compression velocities, the velocity of shocks becomes independent of the degree of crystallinity. This is because for strong shocks the passage of the wave completely melts the crystal structures, rendering the degree of crystallinity irrelevant to the shock speed.

In contrast, Fig. 5(a) also shows that for low compression velocities u_p, the speed of shocks is affected by the degree of crystallinity of the system. This can be better appreciated

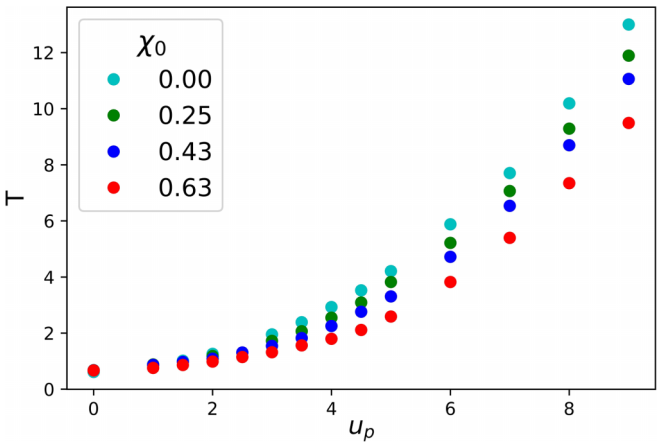

FIG. 4. Temperature increase during shock compression. Temperature of the compressed state as a function of compression speed for systems with different initial crystallinity, denoted as χ_0. Note that the temperature increase is greater in amorphous systems.

in Fig. 5(b), which is an enlargement of the low-velocity-compression region in the v_s-u_p plot, and shows that the shock velocity monotonically increases with the degree of crystallinity of the system. Interestingly, for all the different crystallinities, the shock velocity is proportional (linear) to the compression velocity. From Fig. 5(b), the speed of sound c can be immediately obtained as $c = v_s(u_p \to 0)$. Figure 5(c) shows that the speed of sound continuously grows with increasing crystallinity, which can be roughly approximated by a linear relationship.

Figure 6(a) displays representative velocity profiles for various crystalline systems at low compression velocities ($u_p = 1$). The shock profiles can be effectively approximated by the following phenomenological expression:

$$u(x) = \frac{u_p}{1 + \sum_i \exp[p_i(x - x_0)]}. \tag{3}$$

In this equation, x symbolizes the coordinate in the direction of shock propagation, x_0 denotes the position of the shock wave, and p_i represents fitting parameters utilized to describe the profile (we employ three fitting parameters). This equation serves as an intuitive extension to the commonly employed sigmoid-like function $(x) = 1/[1 + \exp(x)]$, regularly invoked in the examination of symmetric shock wave profiles in systems like gases. However, a more nuanced estimation of variations in attributes such as density, particle velocity, or pressure within asymmetric shock profiles necessitates the use of additional parameters. Equation (3) offers a straightforward and yet precise portrayal of these asymmetric profiles.

With this expression, we can compute the shock's width using the relation [23]

$$\Delta = \frac{u_p}{\max\left(\frac{\partial u}{\partial x}\right)}. \tag{4}$$

In Fig. 6(b), we show the change in the width of the shock as a function of compression velocity for all the systems studied. In general, the width of the shock profiles represents a good measure of how the system dissipates the excess energy due to the passage of the wave [2]. Smaller widths correspond

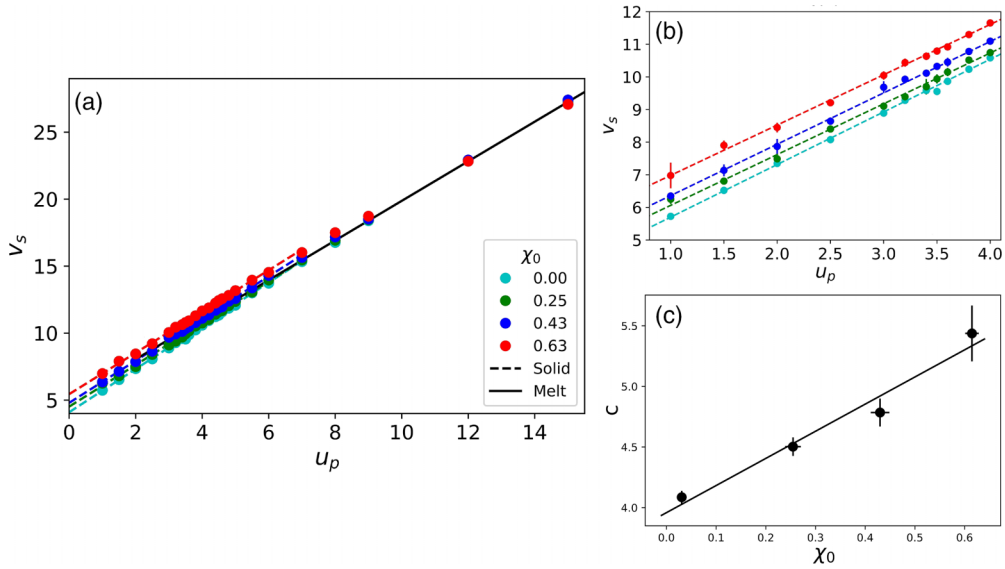

FIG. 5. Relationship between shock velocity and system crystallinity. (a) Velocity of shock waves v_s as a function of compression velocity u_p for systems with varying degrees of crystallinity. (b) Enlarged view of the $v_s - u_p$ relationship at low compression velocities. (c) Variation of the speed of sound c with the degree of crystallinity χ of the system.

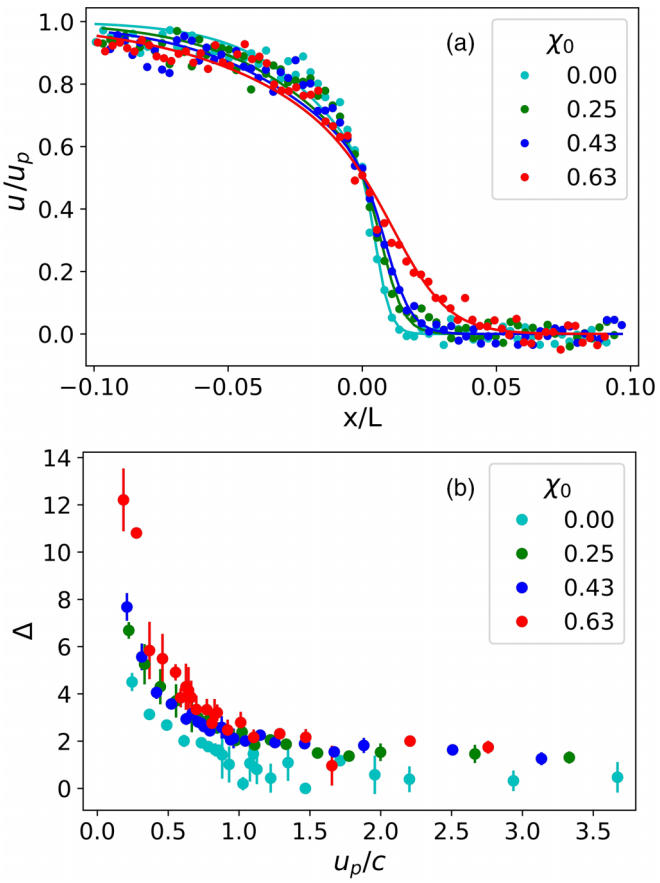

FIG. 6. Relationship between shock width and system crystallinity. (a) Shock wave profiles for systems with varying degrees of crystallinity, compressed at a speed of $u_p = 1$ (front positions were shifted in x for better comparison). (b) Width of the shock wave as a function of compression velocity for systems of different crystallinities.

to stronger shocks, while higher values of width correspond to weaker shocks, where the material has more time to evolve to a new compressed state.

Note that in our crystalline systems the width of shocks increases with the degree of crystallinity, meaning that the presence of hard regions and hard-soft interfaces contributes to the dispersion and effective dissipation of shocks. As expected, in agreement with Fig. 5(a), at high compression velocities, the crystalline structure melts due to the passage of the shock, and all systems display similar widths in the shock profiles.

We also analyze the evolution of crystallinity as shock waves pass through the systems. Figure 7 shows the time evolution of crystallinity in an initial system with a crystallinity

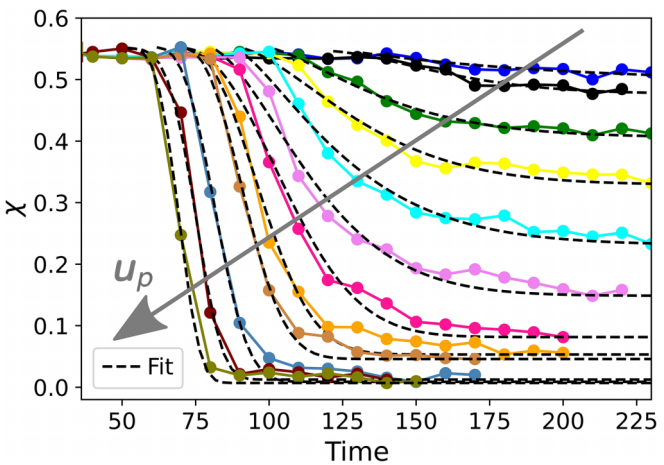

FIG. 7. Evolution of crystallinity. Evolution of crystallinity χ as function of time for different compression velocities, u_p. The arrow points indicates increasing compression velocities ($u_p =$ 1.5, 2, 3, 3.5, 4, 4.5, 5, 5.5, 6, 7, 8, 9). The dashed lines correspond to fittings using Eq. (5).

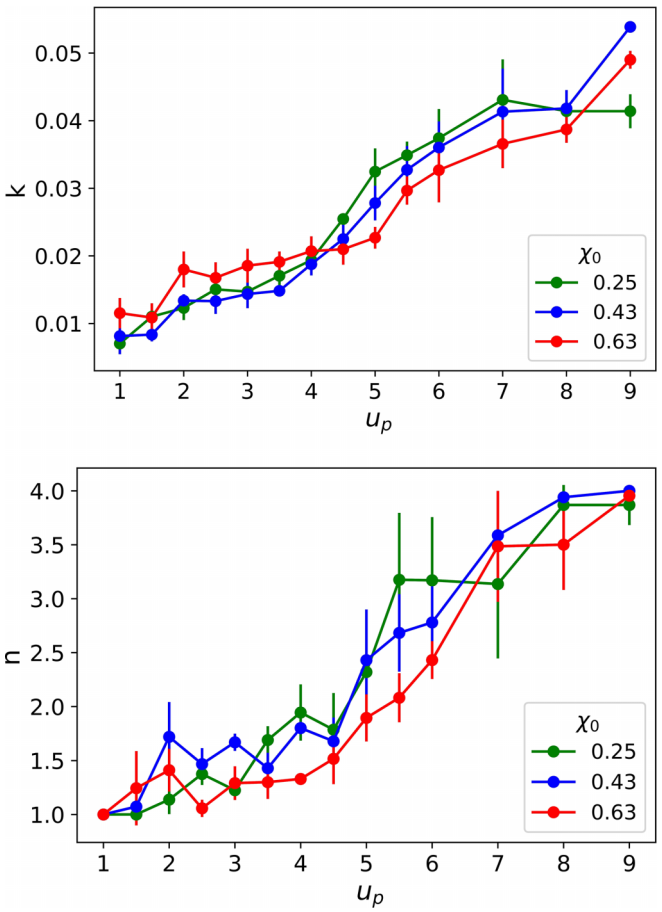

FIG. 8. Avrami coefficients. This figure shows the variation of the Avrami coefficients k (upper panel) and n (bottom panel) as a function of the compression velocity u_p, corresponding to Eq. (5).

of $\chi_0 \sim 0.55$ for different compression velocities. The plot shows that after the passage of the shock, the crystallinity in the system can reduce considerably. Moreover, for strong compression velocities (strong shocks), the final crystallinity approaches zero due to the complete melting of the crystal domains. The time evolution of crystallinity can be approximated by an Avrami-like law [9,24]:

$$\chi = (\chi_0 - \chi_f)\, e^{-k(t-t_0)^n} + \chi_f \tag{5}$$

Here, χ_0 and χ_f are the initial and final crystallinities, respectively, for each compression velocity u_p, and k and n are the Avrami coefficients. In the shock compression simulations, the induction time for the beginning of the transition, t_0, is given by the time it takes the shock front to reach the point x_0 where the evolution of crystallinity is tracked ($t_0 = x_0/v_s$).

Figure 8 shows the variation of the Avrami coefficients k and n as a function of compression velocity for all the systems with different initial crystallinity. In general, both parameters k and n continuously grow with the compression velocity due to distortions and partial or full melting of crystalline structures.

At low compression velocities, the passage of the shock only slightly distorts the crystal domains, and the crystallinity remains almost unchanged (see Fig. 7). Thus, for low compression velocities, the Avrami fits are not very sensitive since

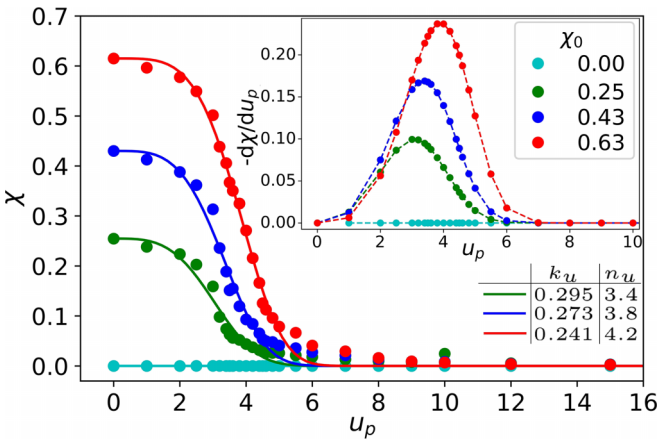

FIG. 9. Final crystallinity. This figure shows the final crystallinity of compressed systems as a function of the compression velocity. The filled lines correspond to a fitting of the values using an Avrami-type function [Eq. (6)]. The inset of the figure shows the negative derivative of the crystallinity of each system as a function of the compression velocity.

almost no phase transition (melting) occurs. In this regime, we observe low values of the Avrami coefficients ($k \sim 0.15$ and $n \sim 1.5$).

In contrast, for high compression velocities, the passage of the shock considerably affects or even fully melts the crystalline domains in the polymer (see Fig. 7). In this regime, both k and n considerably increase with the compression velocity. Note that the n coefficient, which in the Avrami theory is related to the dimensionality of the process, varies from $n \sim 1$ to $n \sim 4$ as we increase the compression velocity. This is because, by increasing u_p, the distortion on the crystal domains grows until the structure is finally fully melted.

Figure 9 shows the remaining value of the crystallinity in each system in the compressed phase, after the passage of the shock wave, as a function of the compression velocity. As discussed above, for low compression velocities the structure is marginally affected, and the system remains with a similar degree of crystallinity. In contrast, as the compression velocity increases, the passage of the wave melts the crystallites, and the crystallinity is reduced considerably.

Note that the melting induced by the fast compression is somewhat related to a melting transition induced by an increase of temperature. Here the continuous motion of the piston injects energy to the system, which produces the phase transition (melting) in the structure.

In analogy with a thermally induced transition, in Fig. 9 we also include the lines corresponding to fitting the numerical results with an Avrami function of the form

$$\chi = \chi_0\, e^{-(k_u u_p)^{n_u}} \tag{6}$$

where k_u, n_p are again the fitting parameters (obtained values in the plot). As expected, for less crystalline systems, the full melt state is reached at lower compression velocities. This can be clearly appreciated for piston velocities $u_p \sim 4$, where χ is higher for materials with initial more crystallinity. Analyzing the k_u parameter, which decreases by increasing the initial crystallinity of the system, we can see how χ decreases

with u_p, where lower k_u means that higher u_p is required to fully melt the system. The parameter n_u, making an analogy with Avrami's equation, would give a representation of the dimensionality and form of the process. The differences in this parameter could correspond to the initial value of crystallinity and crystal size of the system, but in general, we obtain the result that all values are in the same order, $n_u \sim 3$–4. These values for the Avrami exponent compare well with experimental findings in systems like polyethylene or polypropylene, where exponents in the range 2.5–4.0 are typically observed [9,25].

The inset of Fig. 9 shows the change in the degree of crystallinity with the compression speed, $-d\chi/du_p$. Note that the peak of $-d\chi/du_p$ shifts to higher values of u_p for systems with initial higher crystallinity. This is because more crystalline systems require the injection of more energy (compression speed), in order to fully melt the crystal structure.

In our study, we examined the shock compression of semicrystalline polymers, specifically utilizing molecular dynamics (MD) simulations with a coarse-grained model of polyvinyl alcohol (PVA). It is noteworthy that the majority of our analysis is not solely dependent on the type of crystals but is significantly associated with the existence of crystalline regions and interfaces between crystalline and amorphous regions. Consequently, we anticipate observing a comparable phenomenology in other coarse-grained models of semicrystalline polymers [26–29]. Regarding more intricate simulations, such as fully atomistic [30] or density functional theory (DFT) calculations [31], we predict additional energy dissipation mechanisms, primarily in a high compression velocity regime. This is due to the fact that augmenting the degrees of freedom for the molecules also increases the pathways through which energy can be transmitted from the piston to the polymer. Therefore, it is probable that more shock dissipation processes will be observed.

IV. CONCLUSIONS

In this study, we used coarse-grained molecular dynamics simulations to investigate the shock wave response of semicrystalline polymers. The model, which was previously developed to simulate poly(vinyl alcohol), can also be used to model other crystalline systems, such as polyethylene. To accurately control the crystallinity of the systems, we used block copolymer-like chains where only a fraction f of the chain was able to crystallize.

Our results show that the degree of crystallinity affects the speed of sound of the systems, as expected. At low compression velocities, the propagation velocity of shock waves also increases with crystallinity. However, at high compression velocities, the initial crystalline structures melt due to the passage of the shock, and the principal shock features resemble each other, independently of the initial crystallinity.

Overall, our findings indicate that the presence of crystalline regions helps disperse shocks, resulting in a monotonic increase in shock width with the degree of initial crystallinity. The energy injected by the moving piston contributes to the melting of the crystalline regions, and, at some compression velocity, the system becomes completely amorphous after the passage of the shock. The compression velocity required to melt the structures continuously grows with the initial crystallinity of the system.

We were able to analyze the shock-induced melting of the system and found that the evolution of crystallinity qualitatively follows an Avrami law. However, it is far from clear if the shock-induced melting can be entirely described by the Avrami theory. While our findings suggest similarities between the melting induced by fast compression and conventional thermal melting [9,24], one must exercise caution when drawing parallels. Specifically, while the injection of energy due to the passage of the shock front does produce a phase transition (melting) analogous to the effect of increasing temperature, the extent to which the Avrami function can model this remains a subject of investigation. By attempting to fit our numerical results with the Avrami function, we were able to explore the dependence of the degree of crystallinity on compression velocity. This gave us valuable, albeit preliminary, insights into the dimensionality and form of the melting process.

These simulation results highlight the importance of crystalline regions and the presence of amorphous/crystal interfaces in contributing to the dispersion and dissipation of shocks and impact fronts traveling through semicrystalline polymeric materials [7]. This finding is consistent with experimental studies of impact absorption in multiphase polymeric structures [5].

ACKNOWLEDGMENTS

This work was supported by the National Research Council of Argentina, CONICET (PIP 11220200103059CO), the "Fondo para la Investigación Científica y Tecnológica" (FONCYT, Grant No. PICT-2017-3611), and Universidad Nacional del Sur. L.R.G. acknowledges support from by the von Humboldt foundation through the Georg Forster and return fellowships.

[1] Y. B. Zel'Dovich and Y. P. Raizer, *Physics of Shock Waves and High-Temperature Hydrodynamic Phenomena* (Academic, New York, 1967).

[2] M. A. Meyers, *Dynamic Behavior of Materials* (John Wiley & Sons, New York, 1994).

[3] W. J. Carter and S. P. Marsh, Hugoniot equation of state of polymers, Technical Report, Los Alamos National Laboratory, 1995 (unpublished).

[4] R. G. S. Barsoum, *Elastomeric Polymers with High Rate Sensitivity: Applications in Blast, Shockwave, and Penetration Mechanics* (William Andrew, Norwich, NY, 2015).

[5] J.-H. Lee, D. Veysset, J. P. Singer, M. Retsch, G. Saini, T. Pezeril, K. A. Nelson, and E. L. Thomas, High strain rate deformation of layered nanocomposites, Nat. Commun. **3**, 1164 (2012).

[6] A. J. Hsieh, Y.-C. M. Wu, W. Hu, J. P. Mikhail, D. Veysset, S. E. Kooi, K. A. Nelson, G. C. Rutledge, and T. M. Swager, Bottom-up design toward dynamically robust polyurethane elastomers, Polymer **218**, 123518 (2021).

[7] T. C. O'Connor, R. M. Elder, Y. R. Sliozberg, T. W. Sirk, J. W. Andzelm, and M. O. Robbins, Molecular origins of anisotropic shock propagation in crystalline and amorphous polyethylene, Phys. Rev. Mater. **2**, 035601 (2018).

[8] L. Ortellado, D. A. Vega, and L. R. Gómez, Shock melting of lamellae-forming block copolymers, Phys. Rev. E **106**, 044502 (2022).

[9] L. H. Sperling, *Introduction to Physical Polymer Science* (John Wiley & Sons, New York, 2005).

[10] E. Piorkowska and G. C. Rutledge, *Handbook of Polymer Crystallization* (John Wiley & Sons, New York, 2013).

[11] N. Hadjichristidis, S. Pispas, and G. Floudas, *Block Copolymers: Synthetic Strategies, Physical Properties, and Applications* (John Wiley & Sons, New York, 2003).

[12] S. Plimpton, Fast parallel algorithms for short-range molecular dynamics, J. Comput. Phys. **117**, 1 (1995).

[13] D. Reith, H. Meyer, and F. Müller-Plathe, Mapping atomistic to coarse-grained polymer models using automatic simplex optimization to fit structural properties, Macromolecules **34**, 2335 (2001).

[14] H. Meyer and F. Müller-Plathe, Formation of chain-folded structures in supercooled polymer melts, J. Chem. Phys. **115**, 7807 (2001).

[15] H. Meyer and F. Müller-Plathe, Formation of chain-folded structures in supercooled polymer melts examined by MD simulations, Macromolecules **35**, 1241 (2002).

[16] G. Milano and F. Müller-Plathe, Mapping atomistic simulations to mesoscopic models: A systematic coarse-graining procedure for vinyl polymer chains, J. Phys. Chem. B **109**, 18609 (2005).

[17] V. Triandafilidi, J. Rottler, and S. G. Hatzikiriakos, Molecular dynamics simulations of monodisperse/bidisperse polymer melt crystallization, J. Polym. Sci. Part B: Polym. Phys. **54**, 2318 (2016).

[18] Y. R. Sliozberg and J. W. Andzelm, Fast protocol for equilibration of entangled and branched polymer chains, Chem. Phys. Lett. **523**, 139 (2012).

[19] T. Yamamoto, Computer modeling of polymer crystallization–Toward computer-assisted materials' design, Polymer **50**, 1975 (2009).

[20] P. Wen, G. Tao, D. E. Spearot, and S. R. Phillpot, Molecular dynamics simulation of the shock response of materials: A tutorial, J. Appl. Phys. **131**, 051101 (2022).

[21] A. P. Thompson, H. M. Aktulga, R. Berger, D. S. Bolintineanu, W. M. Brown, P. S. Crozier, P. J. in 't Veld, A. Kohlmeyer, S. G. Moore, T. D. Nguyen, R. Shan, M. J. Stevens, J. Tranchida, C. Trott, and S. J. Plimpton, LAMMPS - a flexible simulation tool for particle-based materials modeling at the atomic, meso, and continuum scales, Comput. Phys. Commun. **271**, 108171 (2022).

[22] K. Kadau, T. C. Germann, P. S. Lomdahl, and B. L. Holian, Microscopic view of structural phase transitions induced by shock waves, Science **296**, 1681 (2002).

[23] L. R. Gómez, A. M. Turner, and V. Vitelli, Uniform shock waves in disordered granular matter, Phys. Rev. E **86**, 041302 (2012).

[24] M. Avrami, Kinetics of phase change. I General theory, J. Chem. Phys. **7**, 1103 (1939).

[25] J. N. Hay, Application of the modified Avrami equations to polymer crystallisation kinetics, Br. Polym. J. **3**, 74 (1971).

[26] T. Yamamoto, Molecular dynamics modeling of polymer crystallization from the melt, Polymer **45**, 1357 (2004).

[27] T. Yamamoto, Molecular dynamics of polymer crystallization revisited: Crystallization from the melt and the glass in longer polyethylene, J. Chem. Phys. **139**, 054903 (2013).

[28] P. Yi, C. R. Locker, and G. C. Rutledge, Molecular dynamics simulation of homogeneous crystal nucleation in polyethylene, Macromolecules **46**, 4723 (2013).

[29] L. Zou and W. Zhang, Molecular dynamics simulations of the effects of entanglement on polymer crystal nucleation, Macromolecules **55**, 4899 (2022).

[30] R. H. Gee, N. Lacevic, and L. E. Fried, Atomistic simulations of spinodal phase separation preceding polymer crystallization, Nat. Mater. **5**, 39 (2006).

[31] T. L. Chantawansri, T. W. Sirk, E. F. C. Byrd, J. W. Andzelm, and B. M. Rice, Shock Hugoniot calculations of polymers using quantum mechanics and molecular dynamics, J. Chem. Phys. **137**, 204901 (2012).